Pakistan Veterinary Journal

ISSN: 0253-8318 (PRINT), 2074-7764 (ONLINE)
DOI: 10.29261/pakvetj/2025.255

RESEARCH ARTICLE

Mechanisms of Antibody-Dependent Enhancement of PRRSV Infection: Insights into CR1-like Mediated Pathways in PAMs

Wei Yin[1]*, Qiongyu Li[1], Luyang Xu[1], Jiachen Cheng[1], Zheng Zhang[1], Nan Wang[1], Hongquan Li[1], Kuohai Fan[1], Zhenbiao Zhang[1], Na Sun[1], Panpan Sun[1] and Huizhen Yang[1]

[1]Shanxi Key Laboratory for Modernization of TCVM, College of Veterinary Medicine, Shanxi Agricultural University, Jinzhong, China
*Corresponding author: dkyyinwei@126.com

ARTICLE HISTORY (25-564)

Received: June 29, 2025
Revised: August 22, 2025
Accepted: August 25, 2025
Published online: September 29, 2025

Key words:
Antibody-Dependent Enhancement
CR1-like
PAMs
Porcine
PRRSV

ABSTRACT

Previous research has demonstrated that porcine alveolar macrophages (PAMs) express type I complement receptor molecules (CR1-like). Inhibition of CR1-like activity has been shown to reduce the susceptibility of PAMs to porcine reproductive and respiratory syndrome virus (PRRSV) infection, indicating that CR1-like facilitates PRRSV infection; however, the underlying molecular mechanism remains unclear. This study employed techniques such as immunofluorescence, immunoblotting, scanning electron microscopy, immune blocking, and real-time fluorescence quantification to investigate the molecular mechanism underlying CR1-like mediated PRRSV antibody-dependent enhancement. The findings revealed that the binding of CR1-like to the PRRSV antigen-antibody complex induces dynamic alterations in membrane skeleton proteins, thereby facilitating PRRSV entry into PAMs.

To Cite This Article: Yin W, Li Q, Xu L, Cheng J, Zhang Z, Wang N, Li H, Fan K, Zhang Z, Sun N, Sun P and Yang H 2025. Mechanisms of antibody-dependent enhancement of PRRSV infection: insights into CR1-like mediated pathways in PAMs. Pak Vet J. http://dx.doi.org/10.29261/pakvetj/2025.255

INTRODUCTION

Porcine reproductive and respiratory syndrome (PRRS) is an infectious disease characterized by immunosuppression, attributable to the PRRSV, and has resulted in substantial economic losses within the global swine industry (Li *et al.*, 2024; Sun *et al.*, 2023; Gao *et al.*, 2024). A critical factor contributing to the persistent infection of PRRSV in clinical settings is the virus's antigenic diversity and the phenomenon of antibody-dependent enhancement (ADE) (Zhang *et al.*, 2023; Zhang *et al.*, 2022; Ma *et al.*, 2021). Research has demonstrated that PRRSV ADE can be facilitated by FcγR. Specifically, PRRSV is capable of binding to FcR on PAMs through a sub-neutralizing concentration of antibody Fc terminals, thereby enhancing the virus's ability to attach to the surface of PAMs' membranes, which are the target cells. This interaction subsequently increases the internalization capacity of these target cells for viral particles. Furthermore, it has been observed that FcγR I and FcγR III can suppress the production of IFN-α and TNF-α in PAMs, thereby augmenting PRRSV infection. Concurrently, FcγR IIb can further mediate the occurrence of ADE by recruiting SHIP-1, which enhances PRRSV infection by inhibiting the TBK-1-IRF3-IFN-β signaling pathway (Zhang *et al.*, 2020; Wan *et al.*, 2019).

In addition to the FcR mediated ADE mechanism, complement receptor mediated ADE is also observed in the infection of certain viruses (Prohászka *et al.*, 1997; Nijmeijer *et al.*, 2021; Robinson, 2006; Okuya *et al.*, 2022). The complement system serves as a crucial element of both the innate and adaptive immune responses, augmenting the efficacy of antibodies and phagocytes. Complement receptors are extensively distributed on the surfaces of B lymphocytes, follicular dendritic cells, monocytes, red blood cells, and other cellular membranes (Martínez-Riaño *et al*, 2023; Gasque *et al.*, 1996). Research has demonstrated that when Ebola virus and human parvovirus B19 infect target cells, the complement component C1q can cross link with the C1q receptor on the cell surface through a virus-antibody-C1q complex, thereby facilitating enhanced viral entry into the cells (Takada *et al.*, 2003; Furuyama *et al.*, 2020). The complement component C1q inhibits the ADE effect of flavivirus infection in mice both in vivo and in vitro, in an IgG subclass-specific manner (Von Kietzell *et al.*, 2014; Mehlhop *et al.*, 2007). Furthermore, the complement activation product C3 fragment not only binds to the viral surface protein via antibodies but also promotes the activation of the classical complement pathway. The interaction between the C3 fragment and its corresponding receptor can enhance viral adhesion

through the formation of a virus-antibody-complement complex. This mechanism underlies the ADE phenomenon observed with West Nile virus (Cardosa *et al.*, 1986). The deposition of complement C3 fragments on HIV-1 virus particles can facilitate the interaction between HIV-1 and target cells. These studies are crucial for advancing our understanding of the molecular mechanisms underlying viral infection of host cells (Stoiber *et al.*, 2008). Our prior in vitro experiments demonstrated that when PRRSV-IC was co-incubated with fresh serum, the complement component C3b in the serum sensitized PRRSV-IC through a nucleophilic reaction and interacted with CR1-like receptors on the surface of porcine alveolar macrophages (PAMs), resulting in an antibody-dependent enhancement (ADE) effect. Furthermore, CR1-like receptors were found to cooperate with Fc receptors (FcR) to facilitate PRRSV infection in PAMs (Wang *et al.*, 2019; Zhang *et al.*, 2023). The invasion of host cells by viruses is frequently accompanied by alterations in the actin cytoskeleton dynamics of the host cell membrane. This phenomenon has been observed in various viruses, including flaviviruses, alphaherpesviruses, influenza A virus, and transmissible gastroenteritis virus, which promote actin cytoskeleton polymerization and reorganization to facilitate their infection (Spear and Wu, 2014; Foo and Chee, 2015; Denes *et al.*, 2018; Miranda-Saksena *et al.*, 2018; Bedi and Ono, 2019; Zhang *et al.*, 2019). Previous research has indicated that CR1-like activity influences the level of PRRSV infection in PAMs (Zhang *et al.*, 2023). However, the specific mechanisms underlying the porcine CR1-like-mediated PRRSV-ADE effect, particularly regarding membrane alterations and associated signal transduction pathways, remain unclear. Addressing these scientific questions will contribute to a deeper understanding of the molecular mechanisms involved in the CR1-like-mediated PRRSV-ADE effect.

This experiment employed various techniques to investigate how CR1-like activity regulates PRRSV infection in PAMs, focusing on the link between the actin cytoskeleton and CR1-like-mediated PRRSV-ADE infection, as well as the role of the Rac-1/Cdc 42-PAK 1-LIMK 1-Cofilin signaling pathway. The findings offer new insights and potential targets for PRRSV prevention and control.

MATERIALS AND METHODS

Animals and strains: Healthy 40-day-old Landrace piglets, each weighing approximately 20 kg, were obtained from Taigu County Guannong Agriculture and Animal Husbandry Technology Co, Ltd. Our lab cryopreserved the PRRSV isolate JS-1 with a TCID50 of 10-5.55/mL. The Experimental Animal Ethics Committee of Shanxi Agricultural University approved the experiment (approval number: SXAU-EAW-2021P.DZ.01105001).

Main reagents: 1640 medium, CD64 and CD32 monoclonal antibodies (Functional Grade) were obtained from Semmerfeld Technology Co., Ltd. Protein phosphatase inhibitor mixture, HRP-conjugated Goat Anti-Mouse IgG, and rhodamine-labeled phalloidin were sourced from Beijing Solarbio Technology Co., Ltd. Mouse anti-porcine blue ear monoclonal antibody, Anti-Rac-1/2/3, Anti-Cdc42, Cofilin XP Rabbit mAb, and Phospho-Cofilin Rabbit mAb were acquired from Cell Signaling Technology. Anti-PAK 1 and Anti-PAK 1 (phospho S20) antibodies were purchased from Abcam Technology Co., Ltd. A self-made mouse anti-pig CR1-like monoclonal antibody, with patent number ZL201410308534.0, was developed in the laboratory.

In vitro detection of proliferating PRRSV-infected PAMs: To find the best time to add anti-PRRSV serum after infecting PAMs with PRRSV in vitro, 10 mL blood was centrifuged at 3000 r/min for 15 minutes, and the serum obtained was used for testing. Following the PRRSV vaccine instructions (TJM-F92 strain), 1 mL of live attenuated vaccine was administered. After 21-28 days, blood was collected again, and the serum was separated by centrifugation at 3000 r/min for 15 minutes to obtain anti-PRRSV serum.

A cell suspension with a density of 2.2×10^7/mL was prepared. The PRRSV virus suspension was diluted 1:1000 with 2% 1640 cell culture medium and incubated with PAMs at 37 °C for various times (0, 3, 6, 9, 12, 15, and 18 hours). Cells were collected, centrifuged at 4500 r/min for 5 minutes, and the precipitate was washed with PBS. Then, 500μL of RIPA lysis buffer with 1% protease and phosphatase inhibitors was added, shaken for 15 seconds, sonicated for 15 minutes, and incubated on ice for 40 minutes with shaking every 10 minutes. After the ice bath, cells were centrifuged at 4°C, 12000 r/min for 15 minutes, and the supernatant was collected for total cell protein. The protein concentration was measured using a BCA kit, and 4× protein loading buffer was added to the sample, which was denatured at 95°C for 10 minutes.

The protein sample underwent SDS-PAGE (10% separating, 5% stacking gel), membrane transfer at 200 mA for 1 hour, and blocking with skim milk at room temperature for 2 hours, followed by three 10-minute washes with TBST. The PRRSV N antibody was added and incubated overnight at 4°C. After another three TBST washes, an HRP-labeled secondary antibody diluted in TBST was added and incubated at 37°C for 1 hour. The membrane was washed again with TBST three times for 10 minutes each. The substrate working solution was prepared using Meilunbio's ultra-sensitive ECL luminescent solution. Data analysis was conducted using Image Lab software (Version 6.0, Bio-Rad). Band intensities were quantified from three independent experiments, and results are expressed as mean±SD.

The PRRSV N gene copy number in PRRSV-infected PAMs was measured using qRT-PCR. Total RNA was extracted via the TRIzol method, and gDNA was eliminated. See Table 1 for the reaction system.

The second step involves synthesizing cDNA, as detailed in Table 2. PRRSV N gene primers, designed using the NCBI tool, are listed in Table 3. A recombinant plasmid from our lab served as the template, with PRRSV N-F and PRRSV N-R as primers for qRT-PCR, as outlined in Table 4. Reaction conditions started at 65 °C and ended at 95°C, with 0.5°C increments every 5 seconds. Fluorescence signal0073 were collected to create a melting curve, verifying the N gene's specificity. The recombinant plasmid was diluted from 10^2 to 10^9, and qRT-PCR with PRRSV N-F and PRRSV N-R primers produced amplification and standard curves.

Table 1: The reaction of removing genomic DNA

Regent	Application Amount
Total RNA	1μg
gDNA Eraser	1 μL
5× gDNA Eraser Buffer	2 μL
RNase free ddH_2O	Up to 10 μL
Total Volume	10 μL

Table 2: The reaction of reverse transcription of complementary DNA

Regent	Application Amount
Reaction solution of first step	10 μL
PrimerScript RT Enzyme Mix Ⅰ	1 μL
RT Primer Mix	1 μL
5× PrimerScript Buffer	4 μL
RNase free ddH_2O	4 μL
Total Volume	20 μL

Table 3: Primer sequences for the qRT-PCR

Gene	Primer Sequences(5′-3′)
PRRSV-*N*	F: AGAAGCCCCATTTCCCTCTA R:CGGATCAGACGCACAGTATG

Table 4: qRT-PCR sample addition system

Regent	Volume
2x SYBR Green qPCR Master Mix	10 μL
Forward Primer	1 μL
Reverse Primer	1 μL
cDNA template（10-fold dilution）	1 μL
ddH_2O	7 μL
Total Volume	20 μL

Table 5: Primer sequences for the qRT-PCR

Gene	Primer Sequences(5′-3′)
GAPDH	F:TTGGCTACAGCAACAGGGTG R:CAGGAGATGCTCGGTGTGTT
Rac-1	F:ACCCACAAACAGACGTATTCT R:AGATCAAGCTTCGTCCCCAC
Cdc42	F:CCTTTCTTGCTCGTTGGGAC R:GCACTTCCTTTTGGGTTGAGT
PAK 1	F:CCTGTTGGGAATGGATGGCT R:CTGGGTTCTGAAGCTCTGGG
LIMK 1	F:CCTGGAGGGAAGAACGTATGG R:TGCATTCGCAACACCTGAAG
Cofilin	F:CTGTCTCTGACGGGGTCATC R:ACAAAGGTGGCATAGGGGTC

Amplification efficiency was confirmed with standard curves (R^2> 0.99), and gene copy numbers were determined from three technical replicates per sample. Statistical differences were assessed using one-way ANOVA, with exact p-values provided (significance at P<0.05) and effect sizes calculated to measure the differences' magnitude.

Group and treatment: The experiment consisted of four groups: cell control, PRRSV control, test, and immune blocking. Treatments were as follows: - Cell control group: PAMs were resuscitated, adhered to a monolayer, and cultured with 2 mL of 1640 medium at 37°C and 5% CO_2 for 12 hours. CD16, CD32, and CD64 antibodies (1:1000 dilution) were sequentially added and incubated at 37°C for 2 hours, followed by the addition of 220μL PBS. PRRSV control group: PAMs were treated like cell control group, incubated at 37°C for 2 hours, then the supernatant was removed, and 50μL of $10^{2.55}$/mL PRRSV suspension was added for infection.

In the experimental group, the procedures for cell culture and virus addition were identical to those of the PRRSV control group. Nine hours post-virus addition, 220μL of anti-serum diluted at a ratio of 1:20 and 128.7μL of fresh pig serum were introduced at three-hour intervals, with an additional 128.7μL of fresh pig serum added repeatedly.

In the immune blocking group, PAMs were resuscitated and adhered to a monolayer. CR1-like monoclonal antibody (1:50) and CD16, CD32, CD64 antibodies (1:1000) were added sequentially to each well, with all other procedures matching the experimental group.

Indirect immunofluorescence assay for N gene copy and protein expression: PRRSV was inoculated into each group for 12, 24, 36, and 48 hours. Samples were washed with PBS, fixed with 4% paraformaldehyde, treated with 0.2% Triton X-100, and blocked with 5% BSA. Samples were then incubated with PRRSV-N monoclonal antibody overnight at 4°C, followed by CoraLite® 488-conjugated AffiniPure Goat Anti-Mouse IgG for 1 hour at 37°C. DAPI was then added, and samples were incubated for 5 minutes prior to washing. Cells were resuspended in PBS and analyzed under an inverted fluorescence microscope. Image-Pro Plus 6.0 and Image J software were used to measure the average fluorescence area ratio. Additionally, RNA was extracted to determine the PRRSV N gene copy number in PAMs via qRT-PCR.

Observing cell membrane changes as PAMs capture PRRSV-IC: Samples from each group were collected at various time points. Following cell fixation, membrane permeabilization, and blocking, TRITC-phalloidin (1:200) was added, and the cells were incubated in the dark at 37°C for 1 hour, followed by washing with PBS. First, PRRSV monoclonal antibody was added, followed by CoraLite® 488-conjugated AffiniPure Goat Anti-Mouse IgG. The cells were then incubated in the dark for 1 hour and washed with PBS while protected from light. After DAPI staining, typical visual fields were observed and recorded using an inverted fluorescence microscope.

The sample was fixed in 2.5% glutaraldehyde for 12 hours, rinsed with 0.1 M phosphate buffer (pH 7.0), then fixed in 1% osmic acid for 2 hours and rinsed again. It was dehydrated using a gradient ethanol series (30% to 95%), treated twice with 100% ethanol for 20 minutes each, and dried with a critical point dryer. The sample was mounted on a metal stub with carbon paste, sputter-coated with gold for 30 seconds, and its pseudopod state was examined and recorded using scanning electron microscopy.

Detection of the Rac-1/Cdc42-PAK 1-LIMK 1-Cofilin signaling pathway: Total RNA was extracted from each cell sample group, with primer sequences listed in Table 5. Genes Rac-1, Cdc42, PAK 1, LIMK 1, and Cofilin were analyzed using qRT-PCR, and their relative expression was determined by the $2^{-\Delta\Delta Ct}$ method. Western blotting was employed to detect the proteins Rac-1, Cdc42, PAK 1, phosphorylated PAK 1 (p-PAK 1), LIMK 1, phosphorylated LIMK 1 (p-LIMK 1), Cofilin, and phosphorylated Cofilin (p-Cofilin). Data acquisition was facilitated using Image Lab image analysis software.

Effects of EHoP-016 on PRRSV-IC-Infected PAMs: The experiment involved six groups: cell control, PRRSV control, experimental, immune blocking, EHoP-016 + \PRRSV, and EHoP-016 + PRRSV-IC. The first four groups followed a previous protocol. The new aspect was the addition of EHoP-016 to the last two groups, where PAMs were incubated with

antibodies and serum, followed by 1 mL of 1640 medium with 2.5μM EHoP-016. Samples were collected at 36 hours to measure PRRSV N protein expression.

Statistical analysis: Images were processed with Image-Pro Plus 6.0. T-tests and one-way ANOVA were used for two-group and multi-group comparisons, respectively, in GraphPad Prism 8. Effect sizes were measured using Cohen' s d for t-tests and η^2 for ANOVA by IBM SPSS statistics 31.0. Data are shown as Mean±SEM, with exact p-values reported. Significance is marked as *P<0.05, **P<0.01, ***P<0.001, ****P<0.0001.

RESULTS

The peak time point for PRRSV infection in PAMs: After infecting PAM monolayers with PRRSV, intracellular RNA and whole-cell proteins were collected at 0 (control), 3, 6, 9, 12, 15 and 18 hours post-infection (hpi) to assess PRRSV N gene RNA expression and intracellular PRRSV N protein abundance (15 kDa, with GAPDH (36 kDa) as the internal control; Fig. 1). Western blot results were consistent with RT-PCR trends: PRRSV RNA was detectable at 3 hpi with a relatively low load, followed by rapid proliferation starting at 9 hpi (P< 0.01, vs. 3 hpi). Viral load peaked at 12 hpi (P < 0.001 vs. 9 hpi) and gradually declined at 15 and 18 hpi (Fig. 1). The effect size for PRRSV N gene copy number was 0.701, while for PRRSV N protein gray value, it was 0.913. Based on these temporal dynamics, 9 hpi was selected as the timepoint for administering anti-PRRSV serum and fresh porcine serum.

Identification of PRRSV-ADE cell model: To validate the successful establishment of the PRRSV-ADE cell model, antiserum specific to PRRSV was administered to PAMs nine hours post-infection, in conjunction with fresh porcine serum. The expression levels of the PRRSV N protein were quantitatively assessed using a PRRSV N monoclonal antibody and a CoraLite488-labeled anti-mouse IgG (H+L) fluorescent secondary antibody at 12, 24, 36 and 48 hours following infection (Fig. 2).

The mean fluorescence area ratio for each group was quantified using Image J software. The analysis revealed that the specific fluorescent signal of the PRRSV N protein in the IC group PAMs was significantly greater than that observed in both the virus group and the immune blocking group (P<0.05, Fig. 3-A). qRT-PCR was utilized to quantify the expression levels of the PRRSV N gene at various time intervals. The findings revealed that the intracellular expression of the PRRSV N gene in porcine alveolar macrophages (PAMs) from the IC group was significantly elevated compared to both the viral group and the immunomodulatory blocking group. This suggests that the inhibition of CR1-like activity may affect PRRSV infection in PAMs. Moreover, PRRSV appears to enhance its infection of PAMs via the CR1-like protein present on their surface (P<0.05, Fig. 3-B). The ANOVA for the 12h, 24h, 36h, and 48h groups were 0.976, 0.971, 0.999, and 0.997 in sequence.

PRRSV-IC's impact on PAM cytoskeleton was assessed via indirect immunofluorescence: The impact of PRRSV-IC on the cytoskeleton of porcine alveolar macrophages (PAMs) was evaluated using indirect immunofluorescence. F-actin fluorescent antibody staining and microscopy were performed at 12, 24, 36, and 48 hours post-PRRSV infection to assess morphological changes in PAM membranes. Green fluorescence indicates N protein, red fluorescence represents F-actin, and blue fluorescence (DAPI) labels nuclei; representative images are shown in Figs.4-7.

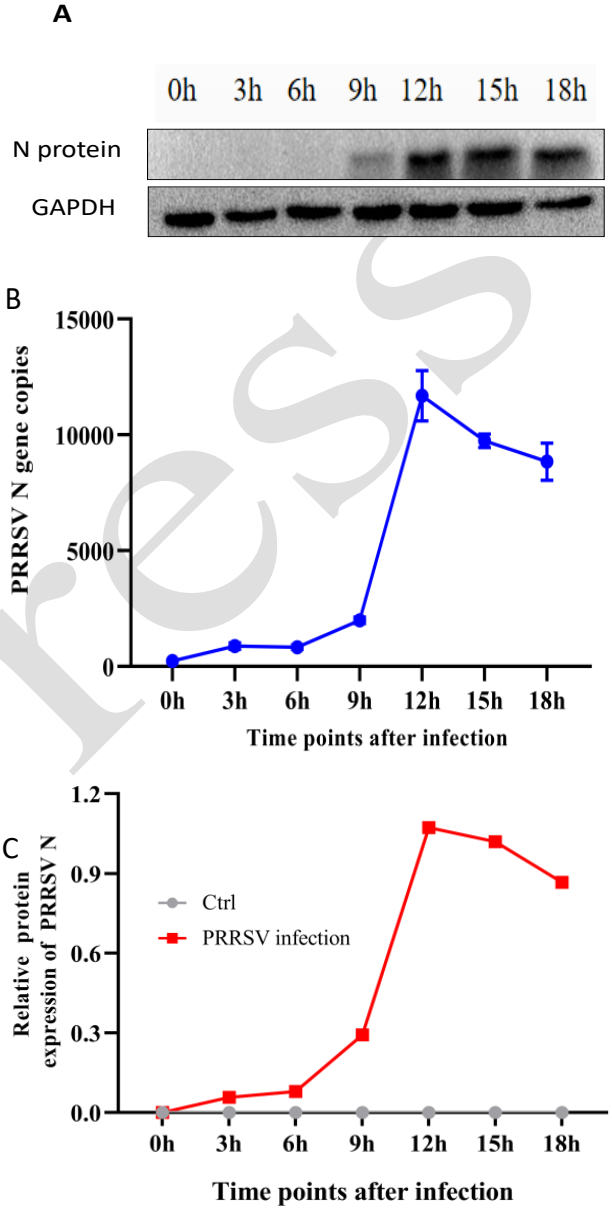

Fig. 1: Effect of PRRSV infection of PAMs at different times on N protein and N gene expression. A: Western blot detection of N protein expression in each group. PRRSV RNA was detectable at 3 h post-infection, with visible N protein bands appearing at 9 h as viral replication accelerated rapidly. The viral load peaked at 12 h and gradually declined at 15 h and 18 h.; B: qRT-PCR analysis of N gene expression. Mean PRRSV N gene copy numbers in PAMs at 0, 3, and 6 h post-infection were 230.4±13.4, 879.3±140.1, and 829.6±95.38, respectively. At 9, 12, 15, and 18 h, copy numbers increased to 1990±141.3, 11686±1090, 9741±284.4, and 8842±800.9, respectively. Statistical analysis by t-tests confirmed that the copy number at 9 h was significantly higher than those at 0, 3, and 6 h. ; C: Western blot analysis of intracellular PRRSV abundance. Viral replication accelerated markedly at 9 h, peaked at 12 h, and gradually decreased at 15 h and 18 h.

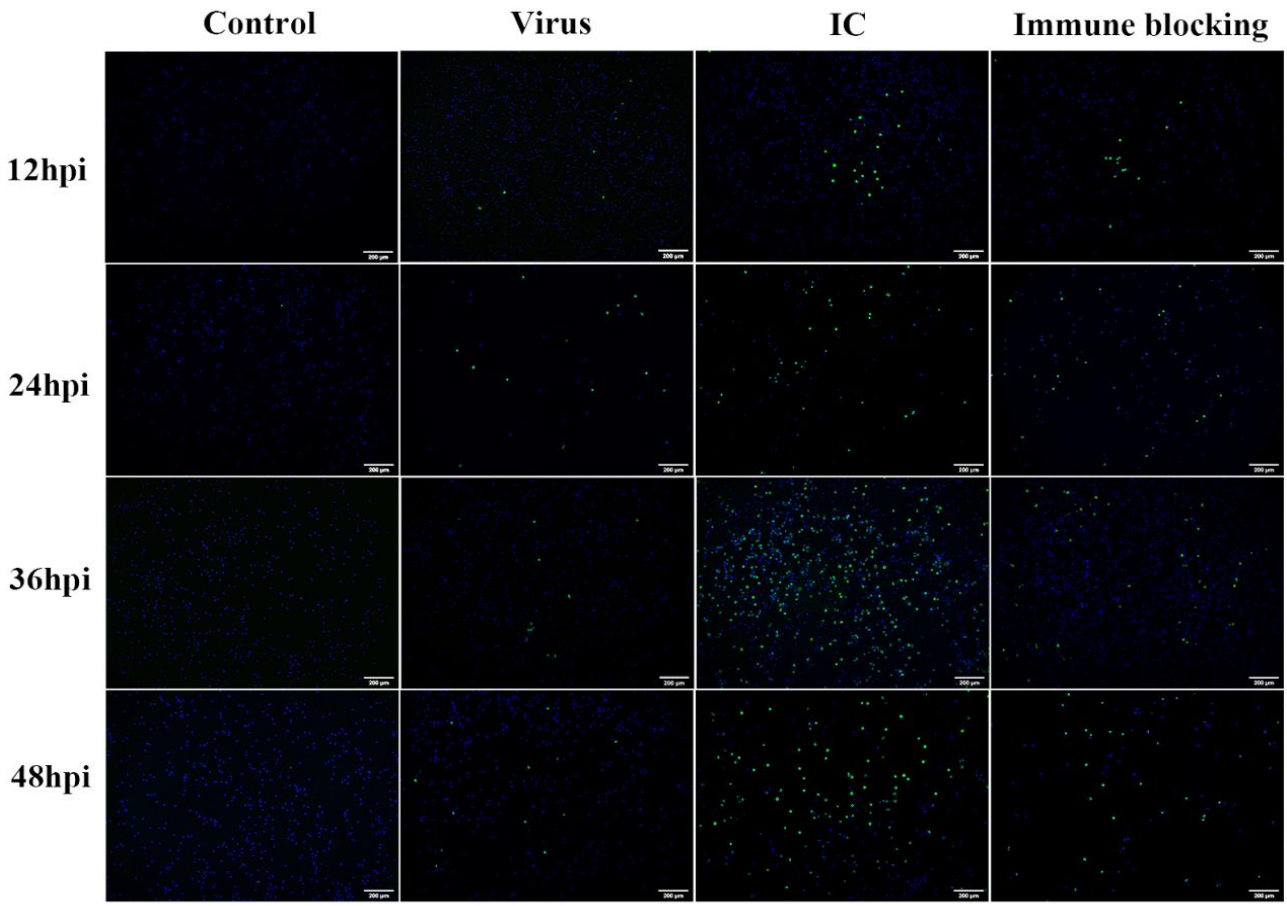

Fig. 2: IFA analysis of viral distribution in control, virus, IC, and immune blocking groups at 12, 24, 36, and 48 hours. Green fluorescence indicates PRRSV N protein, and blue DAPI stains cell nuclei. Scale: 200 μm, magnification 100×.

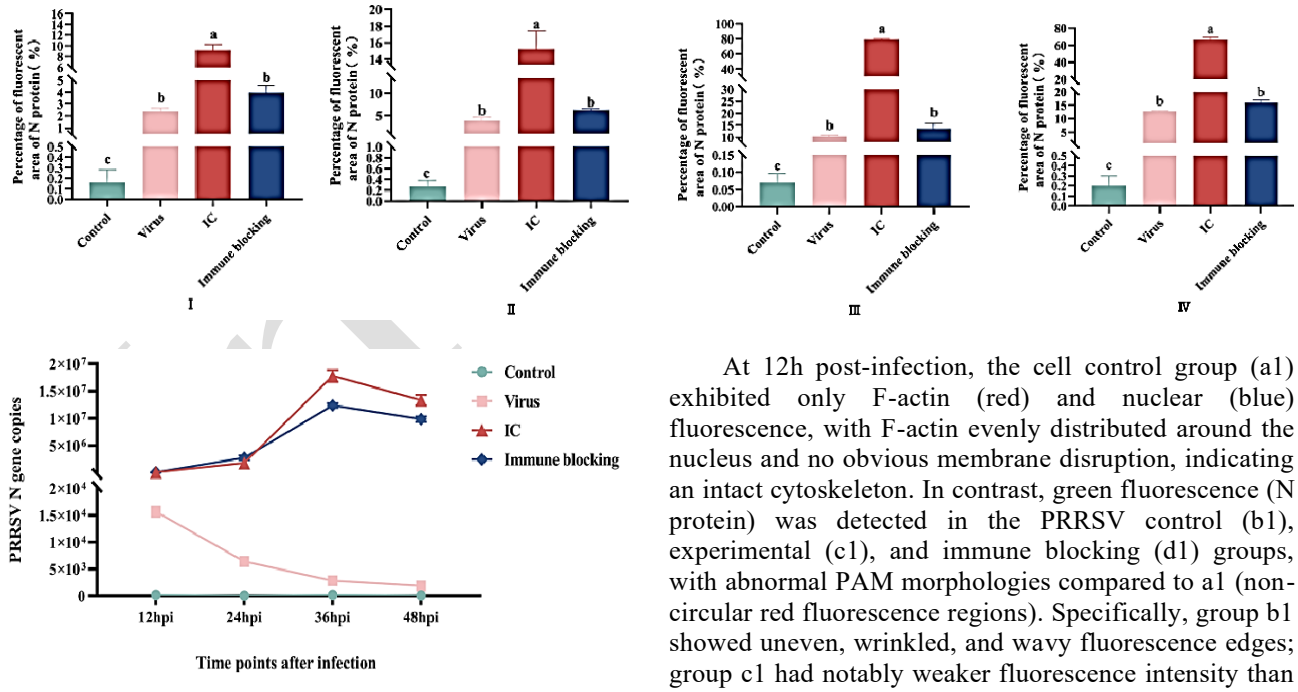

Fig. 3: (A) Average fluorescent area ratio of PRRSV N protein expression analyzed across Image J groups.The nucleus is stained blue by DAPI . Ⅰ, Ⅱ, Ⅲ and Ⅳ are the results of surface virus distribution of PAMs at 12, 24, 36 and 48 hours.(Scale bar = 200 μm, the magnification is 100×). (B) qRT-PCR measured viral copy numbers at 12, 24, 36, and 48 hours post-infection. Statistical significance was determined by one-way ANOVA, with different letters denoting significant differences (P<0.05).

At 12h post-infection, the cell control group (a1) exhibited only F-actin (red) and nuclear (blue) fluorescence, with F-actin evenly distributed around the nucleus and no obvious membrane disruption, indicating an intact cytoskeleton. In contrast, green fluorescence (N protein) was detected in the PRRSV control (b1), experimental (c1), and immune blocking (d1) groups, with abnormal PAM morphologies compared to a1 (non-circular red fluorescence regions). Specifically, group b1 showed uneven, wrinkled, and wavy fluorescence edges; group c1 had notably weaker fluorescence intensity than b1, with uneven edges; group d1 displayed red fluorescence density similar to c1 but a shape closer to b1 (Fig. 4).

At 24h post-infection, the cell control group (a2) maintained intact F-actin distribution and unchanged membranes (Fig. 5). Green fluorescence was observed in groups b2, c2, and d2, with altered morphologies relative

to a2. Group b2 exhibited distinct fluorescence edges and an oval cytoskeleton (a hallmark of viral infection), with reduced red fluorescence boundary density compared to 12 h. Group c2 showed more heteromorphism, lower optical density at fluorescence boundaries than a2 and b2, irregular shapes, and pseudopod-like protrusions. Group d2 had red fluorescence density like c2 but less irregularity than c1 (Fig. 5).

At 36 hours post-infection, only membrane skeleton and nuclear fluorescence were seen in a3 (cell control group), with cells appearing oval and membranes unchanged. Green fluorescence was present in b3 (PRRSV control), c3 (experimental), and d3 (immune blocking) groups, showing different PAM morphologies compared to a3. Group b3 had round membrane skeletons with clearer fluorescence boundaries. Group c3 displayed pseudopods and irregular shapes. Group d3's fluorescence density was like c3, but its irregular shape was less pronounced, as shown in Fig. 6.

At 48h post-infection, the cell control group (a4) retained an oval shape with intact membranes. Green fluorescence was detected in groups b4, c4, and d4. Group b4 showed a round membrane skeleton with reduced red fluorescence intensity; group c4 exhibited significant F-actin depolymerization (dispersed throughout cells) and apoptotic morphology; group d4 had fluorescence intensity similar to c4 but a more oval shape with less irregular fluorescence regions (Fig. 7). These results indicate that PRRSV-IC disrupts the F-actin microfilament cytoskeleton of PAMs.

Ultrastructural alterations in PAM cell pseudopodia caused by PRRSV-IC: It shows each group's pseudopodia features: Group A cells had intact morphology, strong adherence, a rounded shape, and surface flat microvilli. By contrast, Group B cells displayed prominent slender filopodia. Compared with Group B, Group C had both filamentous pseudopodia and flat, short lamellipodia; whereas Group D lacked Group C's lamellipodia and showed no obvious pseudopodia differences from Group B. Consistent with prior reports, PRRSV alone (Group B) induced slender filopodia. Notably, PRRSV-IC (Group C) uniquely induced flat, short lamellipodia—a novel finding not reported in PRRSV-only studies (Fig. 8).

Impact of PRRSV-IC on the Expression of Genes Associated with Actin Cytoskeleton Reorganization in PAMs: The alterations in the expression of genes related to the cell membrane skeleton were assessed using quantitative reverse transcription polymerase chain reaction (qRT-PCR) in the cell control group, PRRSV control group, experimental group, and immune blocking group. These assessments were conducted following the infection of PAMs cells with PRRSV and PRRSV-IC at 12, 24, 36, and 48 hours, as illustrated in Fig. 9.

At 12h post-infection, compared with the PRRSV control group, the experimental group exhibited a significant upregulation of Rac-1, Cdc42, PAK1, LIMK1, and Cofilin (P=0.008, 0.006, 0.005, 0.007, and 0.009, respectively, P<0.01), with fold changes of 1.8, 2.1, 1.9, 2.0, and 2.2. In the immune blocking group, Rac-1, Cdc42,

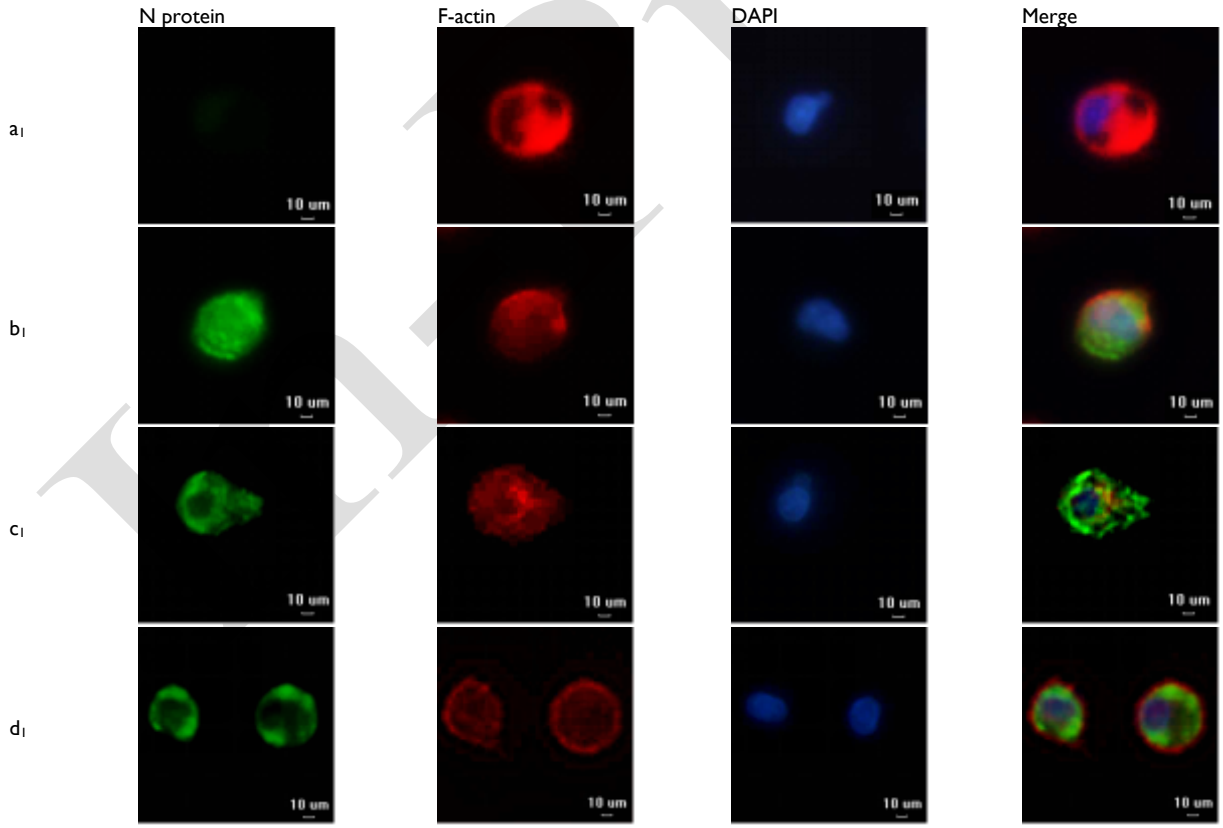

Fig. 4: Results of actin skeleton rearrangement in PAMs cells after 12 h infection with PRRSV and its antigenic antibody complex. The red fluorescence represents rhodamine labeled cyclopeptide; Green fluorescence represents the expression of PRRSV N protein. Nuclei stained blue by DAPI. (Scale bar =10 μm, the magnification is 400 ×).

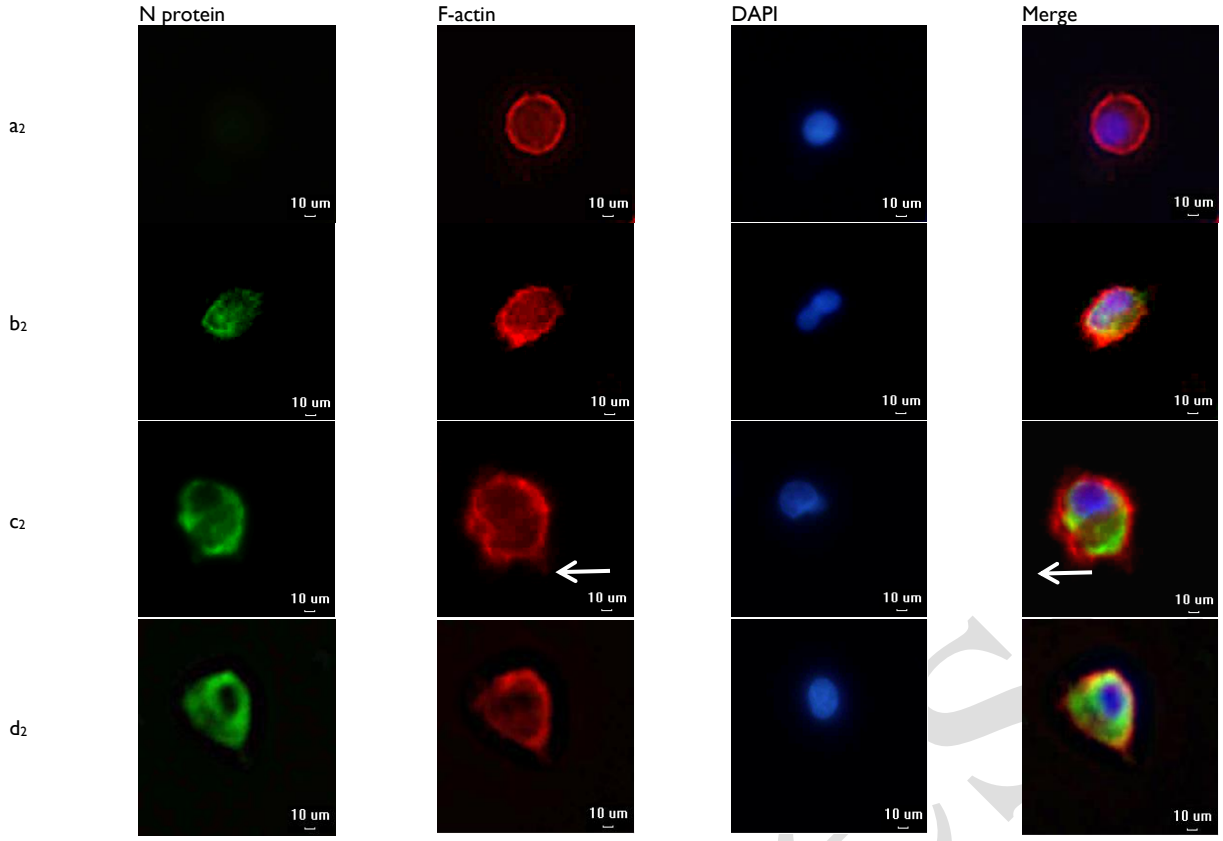

Fig. 5: Results of actin skeleton rearrangement in PAMs cells after 24 h infection with PRRSV and its antigenic antibody complex.The red fluorescence represents rhodamine labeled cyclopeptide; Green fluorescence represents the expression of PRRSV N protein. Nuclei stained blue by DAPI.The white arrows are pseudopodia. (Scale bar =10 μm, the magnification is 400 ×).

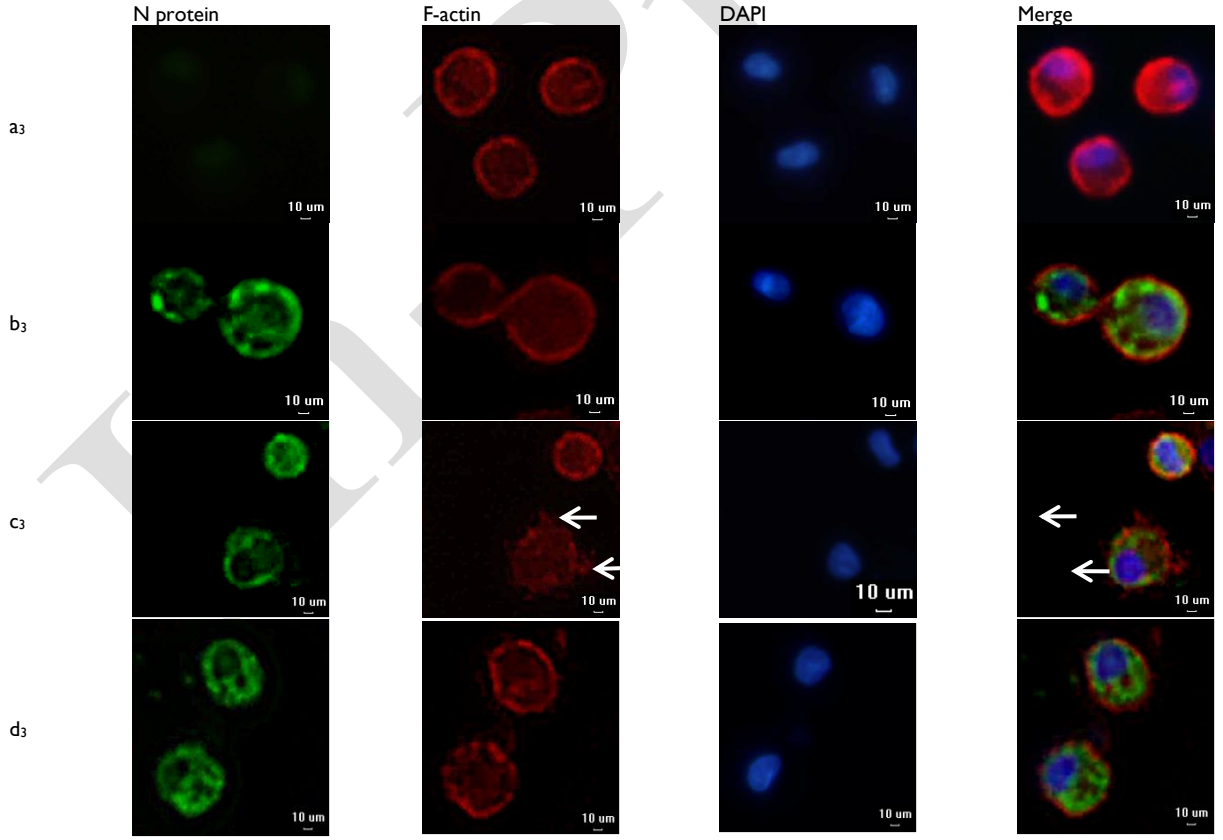

Fig. 6: Results of actin skeleton rearrangement in PAMs cells after 36 h infection with PRRSV and its antigenic antibody complex.The red fluorescence represents rhodamine labeled cyclopeptide; Green fluorescence represents the expression of PRRSV N protein. Nuclei stained blue by DAPI. The white arrows are pseudopodia. (Scale bar =10 μm, the magnification is 400 ×).

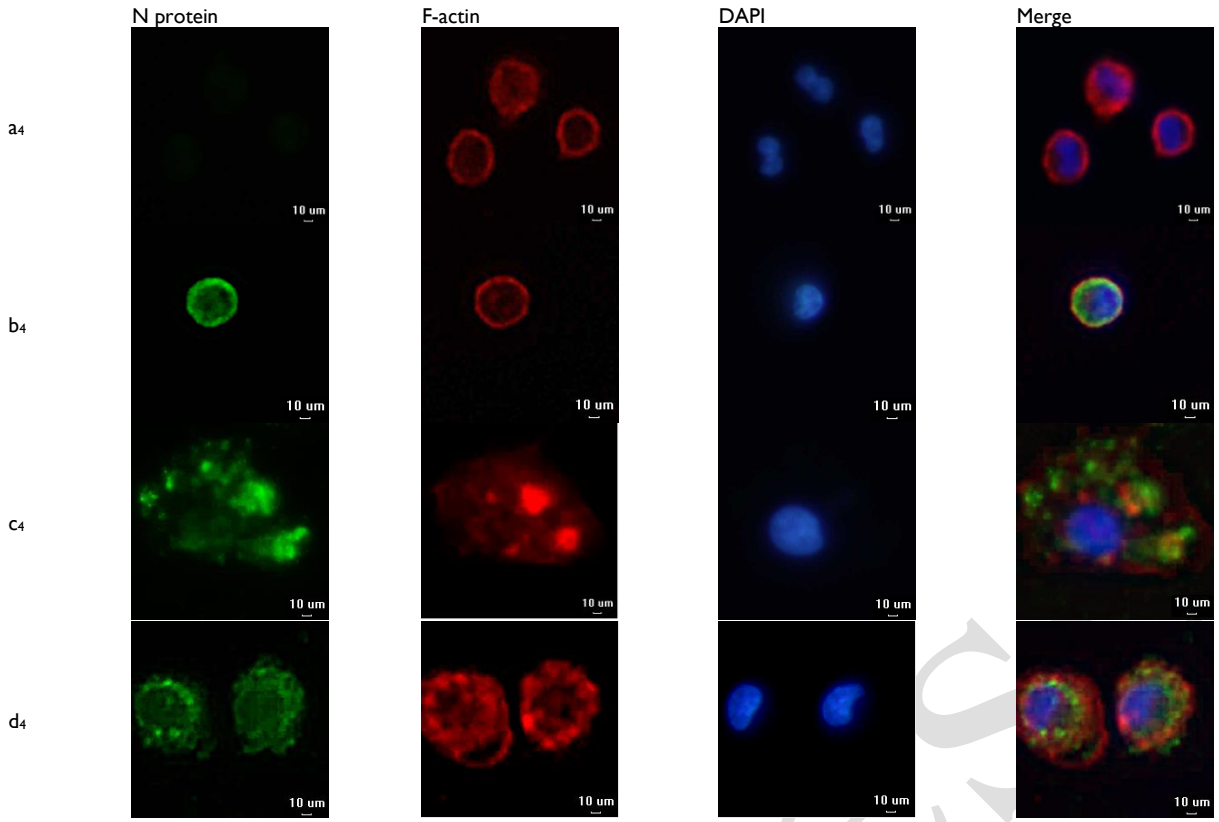

Fig.7: Results of actin skeleton rearrangement in PAMs cells after 48 h infection with PRRSV and its antigenic antibody complex.The red fluorescence represents rhodamine labeled cyclopeptide; Green fluorescence represents the expression of PRRSV N protein. Nuclei stained blue by DAPI. (Scale bar =10 μm, the magnification is 400 ×).

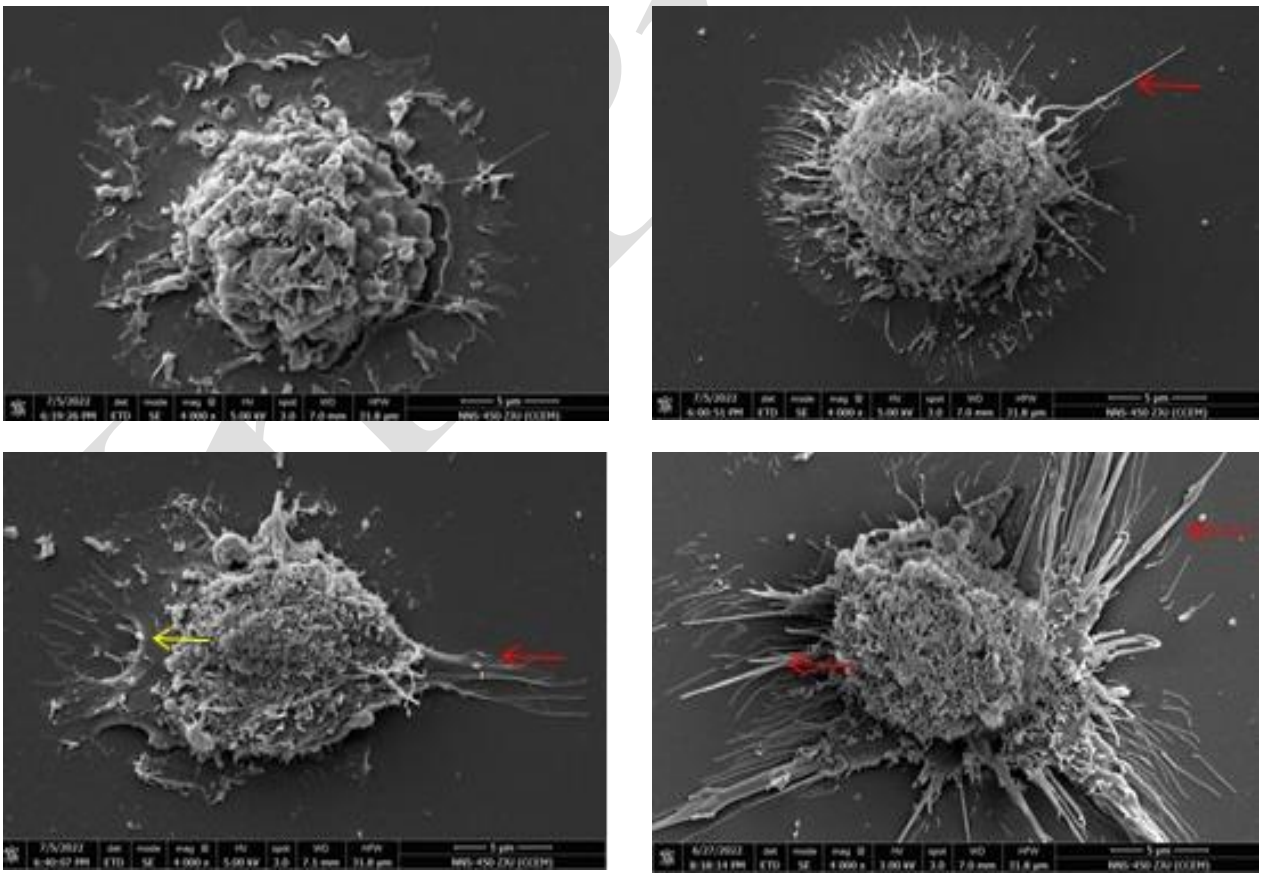

Fig. 8: Electron microscopic observation of PAMs pseudopodia after 36 h infection with PRRSV and its antigen and antibody complex. A: Cell control group; B: PRRSV control group; C:test group; D: immunoblocking group. The red arrow indicates filopodium. The yellow arrow indicates lamellipodium (Voltage: 5000 V, Scale bar =5μM, magnification: 4000×).

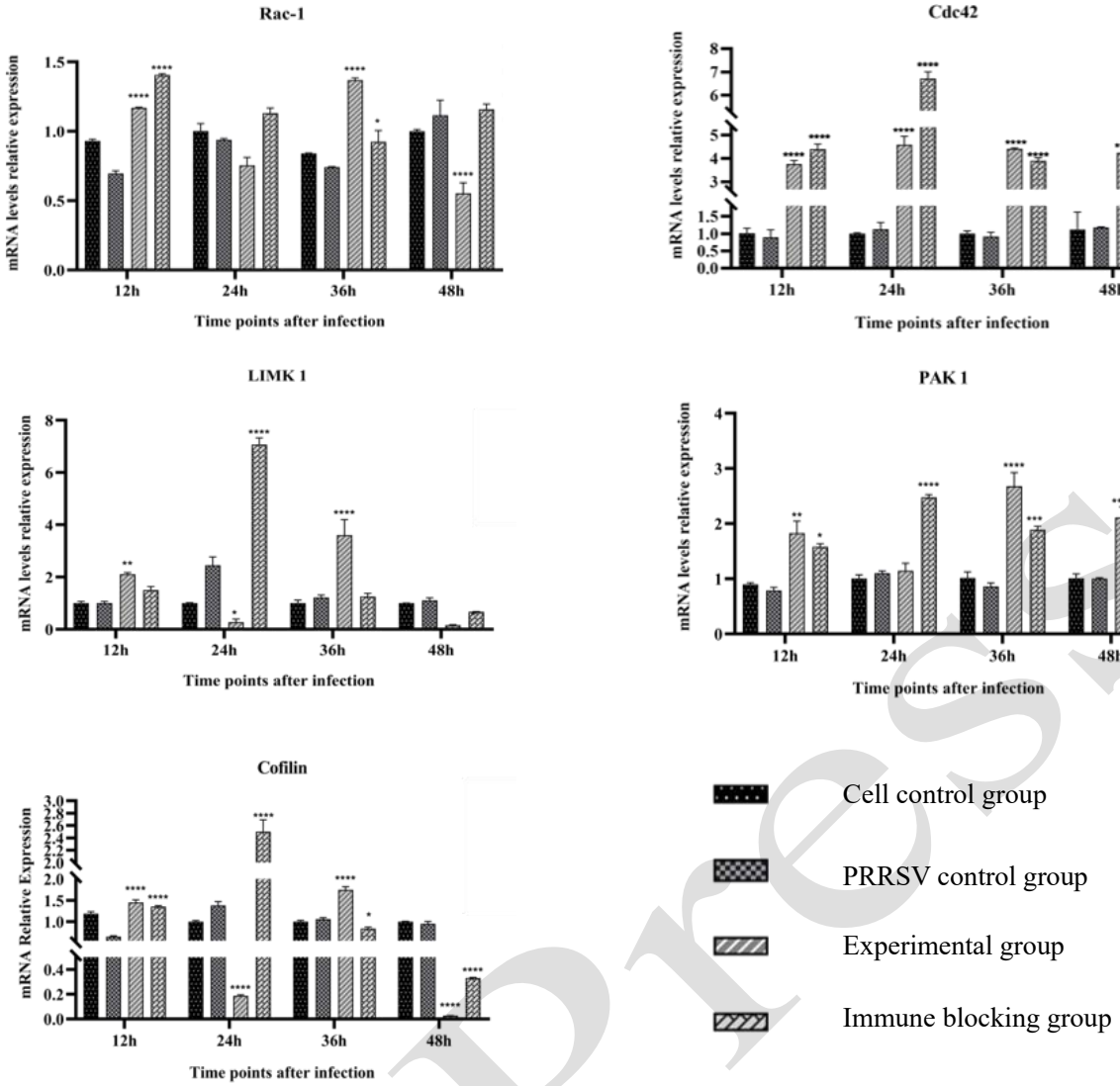

Fig. 9: PRRSV-IC affects actin cytoskeleton-related gene expression in PAMs. qRT-PCR measured Rac-1, Cdc42, PAK1, LIMK1, and Cofilin levels over time and across groups (*P <0.05, **P <0.01, ***P <0.001, ****P <0.0001).

PAK1, and Cofilin were significantly upregulated (P=0.042, 0.038, 0.045, and 0.039, P<0.05; fold changes: 1.3, 1.4, 1.3, and 1.5), while LIMK1 expression remained unchanged (P=0.612, P>0.05).

At 24h post-infection, the experimental group demonstrated a significant downregulation of LIMK1 and Cofilin (P=0.007 and 0.005, P<0.01; fold changes: 0.6 and 0.5) and an upregulation of Cdc42 (P=0.006, P<0.01; fold change: 1.9) compared with the PRRSV control group. Rac-1 and PAK1 expression showed no significant differences (P=0.521 and 0.489, P>0.05).

At 36h post-infection, the experimental group had significantly higher expression of Rac-1, Cdc42, PAK1, LIMK1, and Cofilin than the PRRSV control group (P=0.032, 0.028, 0.035, 0.029, and 0.031, P<0.05; fold changes: 1.6, 1.7, 1.5, 1.6, and 1.7).

At 48 hours post-infection, the experimental group showed significant upregulation of Cdc42 and PAK1 (P=0.008 and 0.007, P<0.05; fold changes: 2.0 and 1.9) and downregulation of Rac-1 and Cofilin (P=0.006 and 0.005, P<0.01; fold changes: 0.5 and 0.4) compared with the PRRSV control group, while LIMK1 expression remained unchanged (P=0.573, P>0.05). In the immune blocking group, Cofilin was significantly downregulated (P=0.007, P<0.01; fold change: 0.4), whereas Cdc42 and PAK1 were upregulated (P=0.008 and 0.009, P<0.01; fold changes: 1.8 and 1.7); Rac-1 and LIMK1 showed no significant differences (P=0.621 and 0.589, P>0.05).

The gene effect sizes of Rac-1, Cdc42, PAK1, LIMK1, and Cofilin were 0.561, 0.632, 0.632, 0.680, and 0.969 in sequence. These findings suggest that PRRSV-IC can modulate actin cytoskeleton-related genes in PAMs, mobilizing intracellular Cofilin to facilitate its efficient entry into host cells.

Effect of PRRSV-IC on actin cytoskeleton signaling pathway in PAMs: This study investigated how PRRSV-IC affects the Rac-1/Cdc42-PAK1-LIMK-Cofilin signaling pathway. Western blot analysis quantified the expression of Rac-1, Cdc42, PAK1, p-PAK1, LIMK1, p-LIMK1, Cofilin, and p-Cofilin in PAMs. As shown in Fig.10, PRRSV and PRRSV-IC differentially regulated these signaling molecules: PRRSV-IC specifically upregulated active (phosphorylated) forms of PAK1 (p-PAK1, 1.5-fold, P=0.003, P<0.01) and LIMK1 (p-LIMK1, 1.4-fold, P=0.004, P<0.01), while total PAK1 and LIMK1 levels remained stable, indicating activation of the Rac-1/Cdc42-PAK1-LIMK axis. Gray values of protein bands were

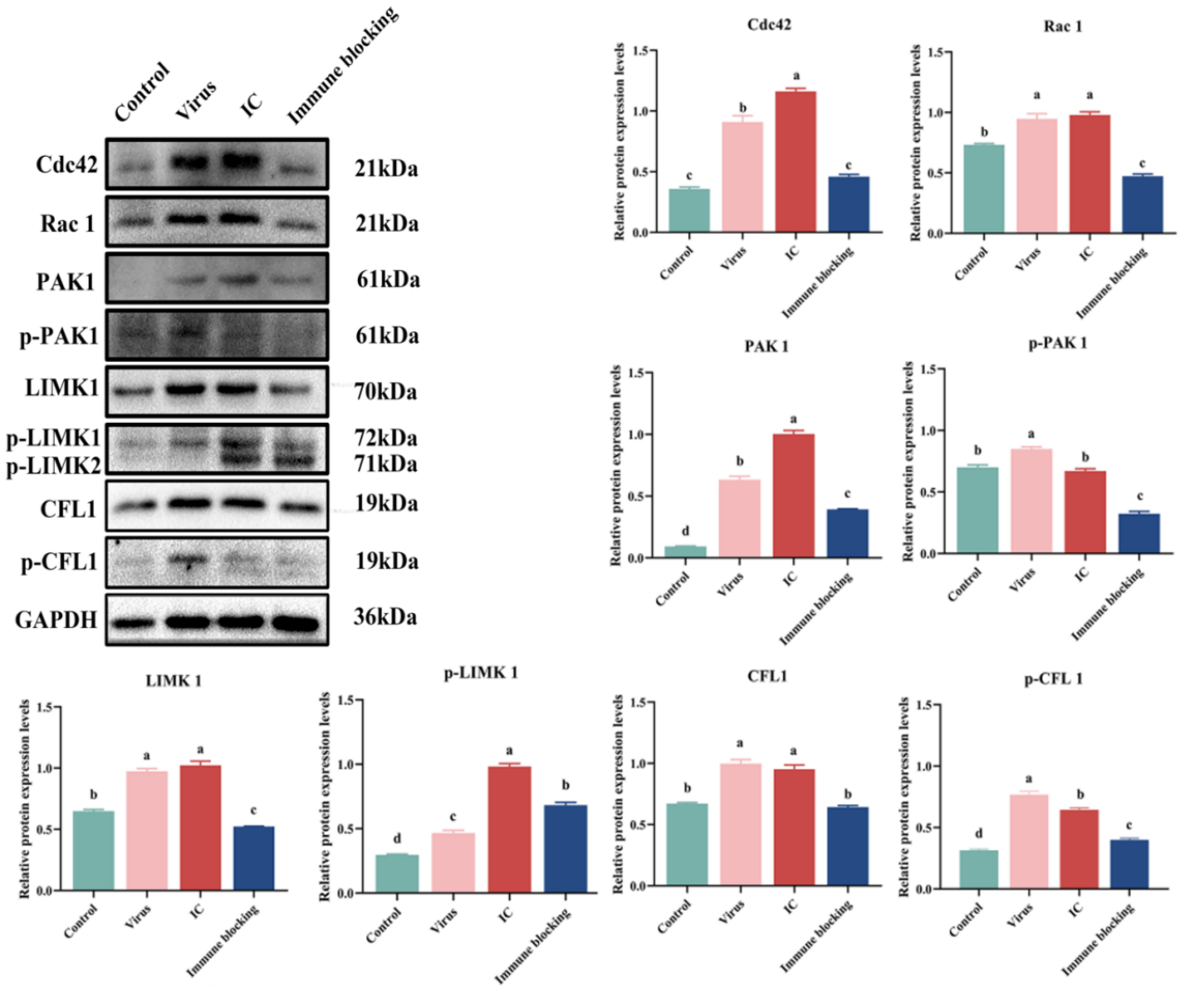

Fig. 10: Expression levels of proteins in Rac-1 / Cdc42-PAK 1-LIMK 1-Cofilin signaling pathway detected by Western blot after PRRSV and PRRSV-IC infection. (A) Expression levels of each protein of Rac-1 / Cdc42-PAK 1-LIMK 1-Cofilin signaling pathway. (B-I) Protein gray level analysis of Rac-1, Cdc42, PAK 1, P-PAK 1, LIMK 1, P-LIMK 1, Cofilin, P-Cofilin. Lowercase letters represent significant difference at 0.05 level in treatment group (P< 0.05); Capital letters represent significant differences at the 0.01 level in the treatment group (P<0.01).

quantified using ImageJ to calculate relative expression. Compared to the PRRSV control group, PRRSV-IC significantly increased Cdc42 (1.2-fold, P=0.002, P<0.01) and Rac1 (1.3-fold, P=0.001, P<0.01) (Fig.10). Relative to the immune blocking group, it also elevated p-Cofilin (1.6-fold, P=0.002). These findings suggest that, at the protein level, PRRSV-IC infected PAMs cells can mobilize intracellular Cofilin, thereby facilitating its efficient entry into host cells through the regulation of actin cytoskeleton rearrangement-related protein expression.The protein effect sizes of Rac-1, Cdc42, PAK1, LIMK1, Cofilin, pCofilin, p-LIMK, p-PAK1, were 0.561, 0.999, 0.997, 0.997, 0.994, 0.993, 0.971, 0.997 in sequence.

The Rac-1 inhibitor EHoP-016 at 5μM significantly reduced cell viability to <70% of the control (P=0.005, P<0.01, partial-η^2=0.998, Fig.11), so 2.5μM was chosen for subsequent experiments. PAMs pre-treated with 2.5μM EHoP-016 were infected with PRRSV or PRRSV-IC, incubated for 36h, and proteins were extracted for Western blot; band intensities were quantified via ImageJ. As shown in Fig.12, the PRRSV N protein in the EHoP-016 + PRRSV-IC group was significantly reduced (1.8-fold, P=0.003, P<0.01, partial-η^2=0.998,) versus the control, our novel finding is that EHoP-016 specifically blocks PRRSV-IC-induced ADE, identifying Rac-1 as a therapeutic target for CR1-like-mediated PRRSV enhancement.

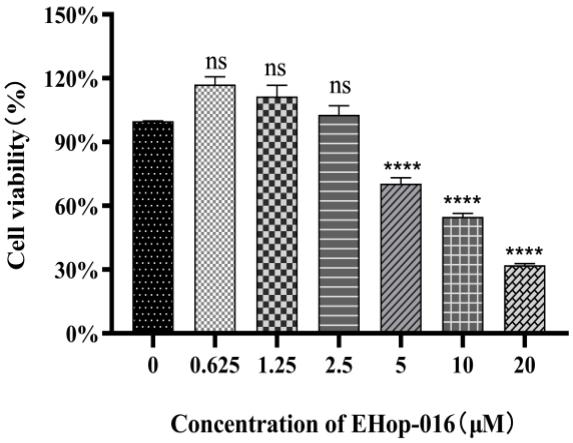

Fig. 11: Effect of different concentrations of EHoP-016 on PAMs activity.**** indicates highly significant differences (P < 0.0001) for each group compared to the control group.

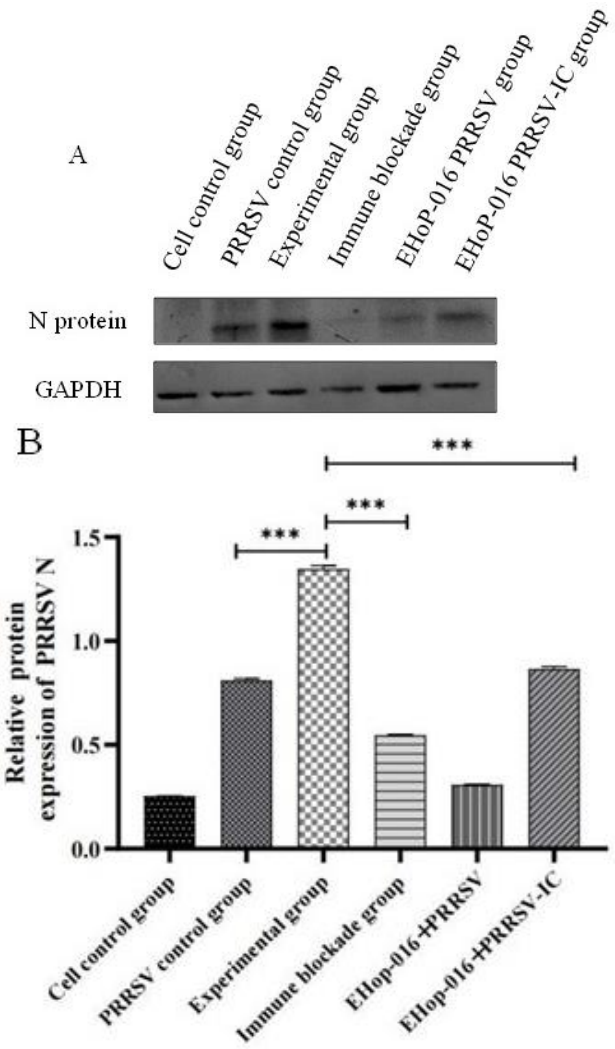

Fig. 12: Effect of EHoP-016 on the expression of PRRSV N protein in PAMs cells infected with PRRSV at 36 h. A: Western blot was used to detect the expression of N protein in each group. B: Gray analysis of PRRSV N protein. *** indicates highly significant difference in the test group compared to EHoP-016+ PRRSV-IC ($P < 0.001$)

DISCUSSION

Several studies have demonstrated that Fc receptor (FcR) molecules on the surface of porcine alveolar macrophages (PAMs) can mediate the antibody-dependent enhancement (ADE) effect of porcine reproductive and respiratory syndrome virus (PRRSV), contributing to the virus's persistent infection in PAMs. Consequently, investigating the underlying mechanisms of the PRRSV-ADE effect holds significant scientific importance. Our prior research identified that complement receptor molecules on the surface of PAMs also facilitate the mediation of PRRSV-ADE; however, the precise molecular mechanisms involved remain elucidated.

Numerous viruses frequently induce dynamic alterations in the actin cytoskeleton of host cell membranes during the infection process. Considering this, the present study investigates the role of the Rac-1/Cdc42-PAK1-LIMK1-Cofilin signaling pathway in the CR1-like-mediated PRRSV-ADE effect. Furthermore, it elucidates the molecular mechanism by which the porcine complement receptor mediates the PRRSV-ADE effect through its influence on the dynamic changes in the actin cytoskeleton.

Effects of CR1-like on PRRSV-infected PAMs: The present study investigates the role of CR1-like in PRRSV-infected PAMs. It is worth noting that critical time points were identified to ensure the scientific rigor of the study. Analysis of the PRRSV N gene copy number and PRRSV N protein expression from 0 to 18 hours post-infection revealed an initial increase followed by a decrease. Notably, at 12 hours post-infection, both the PRRSV N gene copy number and N protein expression peaked, corroborating the researchers' findings (Sun *et al.*, 2016). Nine hours post-PRRSV infection, there was a rapid increase in the PRRSV N gene and protein, suggesting accelerated viral proliferation, which supports the later use of anti-PRRSV serum and pig fresh serum.

Critical novel insights emerge from analyses of ADE mechanisms: Using immunofluorescence and qRT-PCR, we found that fresh serum-sensitized PRRSV-ICs significantly enhanced viral proliferation in PAMs, an effect abrogated by CR1-like blocking. This confirms CR1-like as a mediator of PRRSV ADE in PAMs, a new finding extending previous suggestions of complement involvement in PRRSV ADE（Zhang *et al.*, 2023）.

Comparatively, the mechanism identified in this study differs from ADE in certain other viruses—such as dengue virus and influenza virus—which primarily rely on Fc receptors to exert ADE effects. Instead, it is specifically dependent on CR1-like, in contrast to the Fcγ receptor-dominated ADE seen in these viruses (Lai *et al.*, 2020). Such cross-viral comparison highlights CR1-like-mediated ADE as a distinct pathway in PRRSV, enriching our understanding of viral ADE diversity.

Alterations in cell membrane structure during PRRSV-IC capture by PAMs: Building on the finding that CR1-like enhances PRRSV-ADE, we explored PAM membrane morphological changes during PRRSV-IC capture using SEM and immunofluorescence. Actin cytoskeleton reorganization, critical for pseudopod formation via G/F-actin dynamics (Nie *et al.*, 2021; Dent and Gertler, 2003), generates lamellipodia (branched actin) and filopodia (unbranched actin) (Small *et al.*, 1998; Beli *et al.*, 2008; Innocenti, 2018), a process conserved in ligand-induced responses (Kim *et al.*, 2011) and complement receptor-mediated phagocytosis (Le Cabec *et al.*, 2002).

In our study, PRRSV infection induced F-actin redistribution and pseudopodia formation in PAMs, consistent with actin's role in viral entry reported for other viruses. However, PRRSV-IC (with porcine fresh serum) uniquely triggered concurrent filamentous/lamellipodial pseudopodia, which progressed to cellular disintegration over time—phenotypes absent in PRRSV alone. Critically, blocking CR1-like abrogated lamellipodia, highlighting its specific role in this ADE-associated membrane remodeling.

This contrasts with ADE mechanisms in other viruses, where prominent lamellipodia and similar electron microscopic observations are absent: dengue virus ADE relies on FcγR-mediated actin rearrangement without lamellipodia dominance. Our novel finding is CR1-like's specific induction of lamellipodia in PRRSV-IC capture, linking complement receptor signaling to ADE-associated cytoskeletal changes-extending beyond the known roles of complement receptors in phagocytosis to viral ADE.

Alterations in the microfilament skeleton of PAMs during PRRSV-IC capture: The cytoskeleton is critical for cell morphology, motility, and signal transduction (Ward *et al.*, 2002), with actin polymerization regulated by the Rac-1/Cofilin pathway: Rac-1 activates PAK1 via phosphorylation, which in turn phosphorylates LIMK1; activated p-LIMK1 then phosphorylates Cofilin, inhibiting its actin-depolymerizing activity and promoting pseudopodia formation (Tong *et al.*, 2018; Bryan *et al.*, 2004; Du *et al.*, 2009; Peterburs *et al.*, 2009). As a key member of the ADF/Cofilin family, Cofilin-1 (CFL-1) enhances actin filament turnover through depolymerization/severing and regulates actin dynamics during cellular entry, with its activity controlled by LIMK1/2-mediated phosphorylation at S3 (Chang, 2015; Yang *et al.*, 1998). Additionally, Rho GTPases like Rac-1 (lamellipodia), Cdc42 (filopodia), and RhoA (stress fibers) coordinate cytoskeletal remodeling for cell motility (Aspenström, 2004; Haspel *et al.*, 2021).

This pathway is implicated in viral infections: HIV-1, for instance, activates Rac-1-PAK1-LIMK1-Cofilin via CXCR4/CCR5 binding to facilitate entry and nuclear migration (Vorster *et al.*, 2011). Similarly, dengue virus (DENV) leverages actin remodeling through Rac-1 to enhance endocytic entry during ADE, though its reliance on Cdc42 remains less characterized (Smith *et al.*, 2019). In contrast, our study focuses on PRRSV-IC, demonstrating that it upregulates Rac-1, Cdc42, PAK1, LIMK1, and Cofilin at both mRNA and protein levels (including phosphorylated forms) in PAMs, suggesting a distinct coordination of Rac-1/Cdc42 in PRRSV-IC infection compared to DENV.

While prior studies confirm that Rac-1/Cofilin signaling mediates viral entry (Vorster *et al.*, 2011) and that LIMK/PAK1/Cofilin are involved in cytoskeletal remodeling (Xu *et al.*, 2021; Zhang *et al.*, 2020; Wufuer *et al.*, 2021; Zhang *et al.*, 2020), our work reveals novel insights: PRRSV-IC, unlike parental PRRSV, enhances Rac-1/Cdc42-PAK1-LIMK1-Cofilin activation in PAMs, with this effect linked to CR1-like-mediated infection. Moreover, using the Rac inhibitor EHoP-016 (Montalvo-Ortiz *et al.*, 2012), and demonstrate that blocking Rac-1 reduces PRRSV N protein expression, establishing a causal role of this pathway in PRRSV-IC infection—an interaction not previously reported for PRRSV.

Conclusions: This study elucidates the biological process by which PRRSV-IC phagocytosis is enhanced through alterations in the microfilament cytoskeleton of PAMs, following the interaction of CR1-like molecules on the PAMs membrane surface with sensitized PRRSV-IC. It clarifies the mechanism by which porcine CR1-like facilitates the PRRSV-ADE effect. Under in vitro conditions, CR1-like molecules on the PAMs membrane surface bind to PRRSV-IC sensitized by serum, subsequently inducing the formation of lamellipodia and filopodia on the PAMs cell membrane via the Rac-1/Cdc42-PAK1-LIMK1-Cofilin signaling pathway. This process promotes the phagocytosis of PRRSV-IC by PAMs, thereby contributing to the ADE effect during PRRSV infection of PAMs. The pattern is illustrated in Fig. 13.

Acknowledgements: This work was supported by the National Key Research and Development Program of China (2022YFD1801101), Shanxi Natural Science Research Project (Grant No. 20210302123407), the Shanxi Key Laboratory of Modernization of Traditional Chinese Veterinary Medicine (Grant No. 202104010910015), the Shanxi Agricultural University Doctoral Research Project (Grant No. 2021BQ77), among other funding sources.

Author Contributions: Wei Yin collaboratively conceived and designed the experiments, conducted the inspection analysis and statistical data processing to ensure data quality, contributed to the writing or revision of the draft manuscript, and approved the final version. Qiongyu Li, Luyang Xu, Jiachen Cheng, Zheng Zhang and Nan Wang were responsible for preparing the graphs and contributed to the writing and revision of the draft manuscript. Hongquan Li, Kuohai Fan, Na Sun, Pan Pan Sun, Zhenbiao Zhang and Huizhen Yang participated in the writing and review of the initial draft and gave their approval for the final version. Hongquan Li provided analytical tools and also approved the final draft.

Declaration of interest: The authors declare that they have no competing interests.

REFERENCES

Aspenström P, Fransson A, Saras J, 2004. Rho GTPases have diverse effects on the organization of the actin filament system. Biochem J 377:327-337.

Bedi S, Ono A, 2019. Friend or foe: the role of the cytoskeleton in influenza A virus assembly. Viruses 11:46.

Beli P, Mascheroni D, Xu D, *et al*., 2008. WAVE and Arp2/3 jointly inhibit filopodium formation by entering into a complex with mDia2. Nat Cell Biol 10:849-857.

Bryan B, Kumar V, Stafford LJ, *et al*., 2004. GEFT, a Rho family guanine nucleotide exchange factor, regulates neurite outgrowth and dendritic spine formation. J Biol Chem 279:45824-45832.

Cardosa MJ, Gordon S, Hirsch S, *et al*., 1986. Interaction of West Nile virus with primary murine macrophages: role of cell activation and receptors for antibody and complement. J Virol 57:952-959.

Chang CY, Leu JD, Lee YJ, 2015. The actin depolymerizing factor (ADF)/cofilin signaling pathway and DNA damage responses in cancer. Int J Mol Sci 16:4095-4120.

Denes CE, Miranda-Saksena M, Cunningham AL, *et al*., 2018. Cytoskeletons in the closet-subversion in alphaherpesvirus infections. Viruses 10:79.

Dent EW, Gertler FB, 2003. Cytoskeletal dynamics and transport in growth cone motility and axon guidance. Neuron 40:209-227.

Du D, Pedersen E, Wang Z, *et al*., 2009. Cdc42 is crucial for the maturation of primordial cell junctions in keratinocytes independent of Rac1. Exp Cell Res 315:1480-1489.

Foo KY, Chee HY, 2015. Interaction between flavivirus and cytoskeleton during virus replication. Biomed Res Int 2015:427814.

Furuyama W, Nanbo A, Maruyama J, *et al*., 2020. A complement component C1q-mediated mechanism of antibody-dependent enhancement of Ebola virus infection. PLoS Negl Trop Dis 14:e0008602.

Gao X, You X, Wang G, *et al*., 2024. MiR-320 inhibits PRRSV replication by targeting PRRSV ORF6 and porcine CEBPB. Veterinary Research 55:1.

Gasque P, Chan P, Mauger C, *et al*., 1996. Identification and characterization of complement C3 receptors on human astrocytes. J Immunol 156:2247-2255.

Haspel N, Jang H, Nussinov R, 2021. Active and inactive Cdc42 differ in their insert region conformational dynamics. Biophys J 120:306-318.

Innocenti M, 2018. New insights into the formation and the function of lamellipodia and ruffles in mesenchymal cell migration. Cell Adh Migr 12:401-416.

Kim KB, Yi JS, Nguyen N, *et al*., 2011. Cell-surface receptor for complement component C1q (gC1qR) is a key regulator for lamellipodia formation and cancer metastasis. J Biol Chem 286:23093-23101.

Lai YC, Chao CH and Yeh TM, 2020. Roles of macrophage migration inhibitory factor in dengue pathogenesis: from pathogenic factor to therapeutic target. Microorganisms 8:891

Le Cabec V, Carréno S, Moisand A, *et al*., 2002. Complement receptor 3 (CD11b/CD18) mediates type I and type II phagocytosis during nonopsonic and opsonic phagocytosis, respectively. J Immunol 169:2003-2009.

Li G, Zheng Y, Luo Q, *et al*., 2024. Research progress on the NSP10 protein of porcine reproductive and respiratory syndrome virus. Microorganisms 12:553.

Ma J, Ma LL, Yang MT, *et al*., 2021. The function of the PRRSV-host interactions and their effects on viral replication and propagation in antiviral strategies. Vaccines 9:364.

Martínez-Riao A, W S, Boeing S, *et al*., 2023. Long-term retention of antigens in germinal centers is controlled by the spatial organization of the follicular dendritic cell network. Nat Immunol 24:1281-1294.

Mehlhop E, Ansarah-Sobrinho C, Johnson S, *et al*., 2007. Complement protein C1q inhibits antibody-dependent enhancement of flavivirus infection in an IgG subclass-specific manner. Cell Host Microbe 2:417-426.

Miranda-Saksena M, Denes CE, Diefenbach RJ, *et al*., 2018. Infection and transport of herpes simplex virus type 1 in neurons: role of the cytoskeleton. Viruses 10:92.

Montalvo-Ortiz BL, Castillo-Pichardo L, Hernández E, *et al*., 2012. Characterization of EHoP-016, novel small molecule inhibitor of Rac GTPase. J Biol Chem 287:13228-13238.

Nie Y, Hui L, Guo M, *et al*., 2021. Rearrangement of actin cytoskeleton by Zika virus infection facilitates blood-testis barrier hyperpermeability. Virol Sin 36:692-705.

Nijmeijer BM, *et al*., 2021. HIV-1 subverts the complement system in semen to enhance viral transmission. Mucosal Immunol 14:743-750.

Okuya K, Hattori T, Saito T, *et al*., 2022. Multiple Routes of Antibody-Dependent Enhancement of SARS-CoV-2 Infection. Microbiol Spectr 10:e01553-21.

Peterburs P, Heering J, Link G, *et al*., 2009. Protein kinase D regulates cell migration by direct phosphorylation of the cofilin phosphatase slingshot 1 like. Cancer Res 69:5634-5638.

Prohászka Z, Nemes J, Hidvégi T, *et al*., 1997. Two parallel routes of the complement-mediated antibody-dependent enhancement of HIV-1 infection. AIDS 11:949-958.

Robinson WE, 2006. Mechanism for complement-mediated, antibody-dependent enhancement of human immunodeficiency virus type 1 infection in MT2 cells is enhanced entry through CD4, CD21, and CXCR4 chemokine receptors. Viral Immunol 19:434-447.

Small JV, Rottner K, Kaverina I, *et al*., 1998. Assembling an actin cytoskeleton for cell attachment and movement. Biochim Biophys Acta 1404:271-281.

Spear M, Wu Y, 2014. Viral exploitation of actin: force-generation and scaffolding functions in viral infection. Virol Sin 29:139-147.

Stoiber H, Soederholm A, Wilflingseder D, *et al*., 2008. Complement and antibodies: a dangerous liaison in HIV infection? Vaccine 26:179-185.

Sun N, Sun P, Lv H, *et al*., 2016. Matrine displayed antiviral activity in porcine alveolar macrophages co-infected by porcine reproductive and respiratory syndrome virus and porcine circovirus type 2. Sci Rep 6:24401.

Sun Q, Xu H, An T, *et al*., 2023. Recent progress in studies of porcine reproductive and respiratory syndrome virus 1 in China[J]. Viruses, 15(7): 1528.

Takada A, Feldmann H, Ksiazek TG, *et al*., 2003. Antibody-dependent enhancement of Ebola virus infection. J Virol 77:7539-7544.

Tong H, Qi D, Guan X, *et al*., 2018. c-Abl tyrosine kinase regulates neutrophil crawling behavior under fluid shear stress via Rac/PAK/LIMK/cofilin signaling axis. J Cell Biochem 119:2806-2817.

Von Kietzell K, Pozzuto T, Heilbronn R, *et al*., 2014. Antibody-mediated enhancement of parvovirus B19 uptake into endothelial cells mediated by a receptor for complement factor C1q. J Virol 88:8102-8115.

Vorster PJ, Guo J, Yoder A, *et al*., 2011. LIM kinase 1 modulates cortical actin and CXCR4 cycling and is activated by HIV-1 to initiate viral infection. J Biol Chem 286:12554-12564.

Wan B, Chen X, Li Y, *et al*., 2019. Porcine FcγRIIb mediated PRRSV ADE infection through inhibiting IFN-β by cytoplasmic inhibitory signal transduction. Int J Biol Macromol 138:198-206.

Wang C, Yin W, Fan KH, *et al*., 2019. Identification of complement-like receptor molecules on the membrane surface of pig alveolar macrophages. Heilongjiang Animal Husbandry and Veterinary Medicine (first half of the month) 4:13-17.

Ward Y, Yap SF, Ravichandran V, *et al*., 2002. The GTP binding proteins Gem and Rad are negative regulators of the Rho-Rho kinase pathway. J Cell Biol 157:291-302.

Wufuer R, Ma HX, Luo MY, *et al*., 2021. Downregulation of Rac1/PAK1/LIMK1/cofilin signaling pathway in colon cancer SW620 cells treated with Chlorin e6 photodynamic therapy. Photodiagn Photodyn 33:102143.

Xu J, Ma X, Yang H, *et al*., 2021. MiR-509-3p induces apoptosis and affects the chemosensitivity of cervical cancer cells by targeting the RAC1/PAK1/LIMK1/cofilin pathway. Chem Pharm Bull (Tokyo) 69:325-332.

Yang N, Higuchi O, Ohashi K, *et al*., 1998. Cofilin phosphorylation by LIM-kinase 1 and its role in Rac-mediated actin reorganization. Nature 393:809-812.

Zhang L, Li W, Sun Y, *et al*., 2020. Antibody-mediated porcine reproductive and respiratory syndrome virus infection downregulates the production of interferon-α and tumor necrosis factor-α in porcine alveolar macrophages via Fc gamma receptor I and III. Viruses 12:187.

Zhang LJ, Feng X, Wang HD, *et al*., 2023. Antibody-dependent enhancement of porcine reproductive and respiratory syndrome virus infection downregulates the levels of interferon-gamma/lambdas in porcine alveolar macrophages in vitro. Front Vet Sci 10:1150430.

Zhang LJ, Wang HD, Li W, *et al*., 2022. Activating Fc gamma receptors and viral receptors are required for antibody-dependent enhancement of porcine reproductive and respiratory syndrome virus infection. Vet Sci 9:470.

Zhang M, Chen L, Liu Y, *et al*., 2020. Sea cucumber Cucumaria frondosa fucoidan inhibits osteosarcoma adhesion and migration by regulating cytoskeleton remodeling. Oncol Rep 44:469-476.

Zhang S, Shi W, Hu W, *et al*., 2020. DEP domain-containing protein 1B (DEPDC1B) promotes migration and invasion in pancreatic cancer through the Rac1/PAK1-LIMK1-Cofilin1 signaling pathway. Onco Targets Ther 13:1481-1496.

Zhang Y, Gao W, Li J, *et al*., 2019. The role of host cytoskeleton in flavivirus infection. Virol Sin 34:30-41.

Zhang Z, Sun YC, Fan KH, *et al*., 2023. Effect of PAMs immunoadhesion receptor CR1-like on PRRSV infection. J Shanxi Agri Uni (Natural Science Edition) 43:100-110.